Research paper

# Quantifying the late-to post-Variscan pervasive heat flow, central Netherlands, Southern Permian Basin

Damien Bonté[a,*], Jeroen Smit[a], Rader Abdul Fattah[b], Susanne Nelskamp[b], Sierd Cloetingh[a], Jan-Diederik van Wees[a,b]

[a] Faculty of Geoscience, Utrecht University, Utrecht, the Netherlands
[b] TNO – Geological Survey of the Netherlands, Princetonlaan 6, 3584 CB, Utrecht, the Netherlands

A B S T R A C T

The Southern Permian Basin is marked by significant Latest Carboniferous-Early Permian magmatism attributed to mantle plume emplacement. This intense magmatic activity is commonly assumed to have impacted the heat flow in this area. In the central Netherlands a large number of wells show evidence of magmatic activity dated as Permo-Carboniferous. In addition, high maturity values have been measured for the Carboniferous and below. Theoretical models for tectonic heat flow and maturity evolution presented in this paper show that mantle upwelling, underplating, and intrusions have a significant effect on maturity-depth trends.

Tectonic modelling of five selected wells shows that tectonic subsidence and exhumation can be correlated with a significant heat flow pulse at Latest Carboniferous-Early Permian time. This could well explain the widespread elevated maturity/depth gradient in Carboniferous rocks. Quantitative assessment of heat flow, based on a model of mantle plume emplacement, shows that mantle upwelling and underplating at the base of the crust, proposed by previous studies, provides insufficient heat flow to explain strongly elevated maturity-depth trends. In contrast, widespread Permo-Carboniferous calc-alkaline magmatism at shallow crustal levels provides a mechanism for elevated heat flow with a regional impact, consistent with observed high maturity-depth trends. The model and maturity data demonstrate that elevated maturity at shallow burial-depth levels of 500–1000 m is probably sited in the gas window during a heat pulse, occurring at Late Carboniferous times.

## 1. Introduction

The Southern Permian Basin in Northern Europe is marked by significant magmatism around the Carboniferous-Permian boundary in the aftermath of the Variscan orogeny (Ziegler et al., 2006; Timmerman, 2004; Torsvik et al., 2008; Pharaoh et al., 2010). Basin analysis studies have shown that magmatism plays a key role in the evolution of accommodation space in the Southern Permian Basin (van Wees et al., 2000). Significant quantities of intrusive and extrusive rocks have been recorded in different areas in the Southern Permian Basin area and its margins (e.g., Heeremans et al., 2004, Fig. 1). Theoretical models for tectonic heat flow and maturity evolution (e.g., Allen and Allen, 2005; Fjeldskaar et al., 2003; van Wees et al., 2009; Cloetingh et al., 2010) show that maturity-depth trends can be impacted by mantle upwelling, underplating, and magmatic activity.

To assess the impact of a Permo-Carboniferous heat pulse on maturity evolution, we have used a numerical modelling approach. To this aim, we have made a selection of wells in the Texel IJsselmeer High

(Fig. 2). This area has been selected as it allows to characterise the heat pulse related to magmatic activity at the Permo-Carboniferous without interference of younger events. The modelling method that we used was developed for the prediction of tectonic heat flows and associated maturity and is also capable of taking into account the effects of mantle upwelling and underplating (van Wees et al., 2009; Hirsch et al., 2010; Corver et al., 2011; Beglinger et al., 2012). In the model the tectonostratigraphy is constrained by wells and related to basin history. Due to the local and regional nature of the datasets available for this study, we adopt the stratigraphic framework utilised in the literature on this area. For clarity, Fig. 3 allows comparison and calibration with international chronostratigraphic nomenclature. We model the basin evolution by using an inversion method that is constrained by the structure of the sedimentary basin and underlying lithosphere, and affected by the deformation of the lithosphere and magmatic intrusions and underplating. Burov and Cloetingh (2009) and Koptev et al. (2017) have demonstrated the intrinsic link between plume emplacement and intraplate stress regime in the deformation and thermal perturbation of the
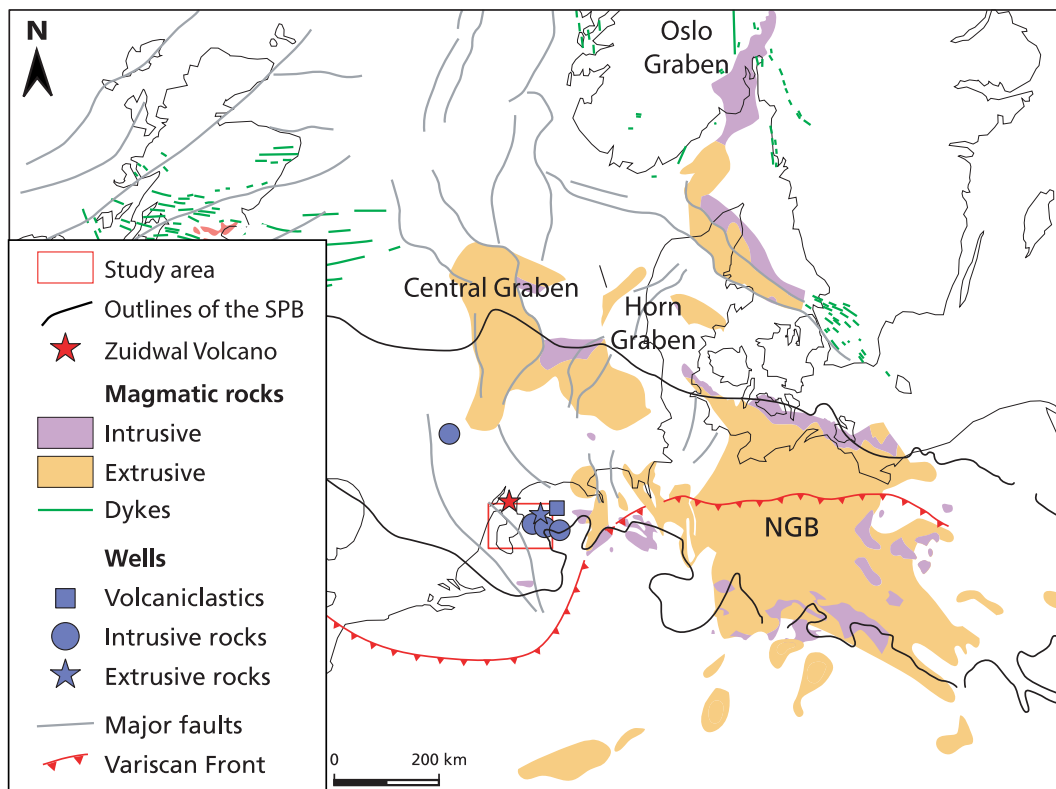
---

**Fig. 1.** Location of magmatic events in the Southern Permian Basin Area during the Late Carboniferous and the Permian, with location of volcanic occurences (source: van Bergen and Sissingh, 2007). NGB: North German Basin. SPB: Southern Permian Basin.
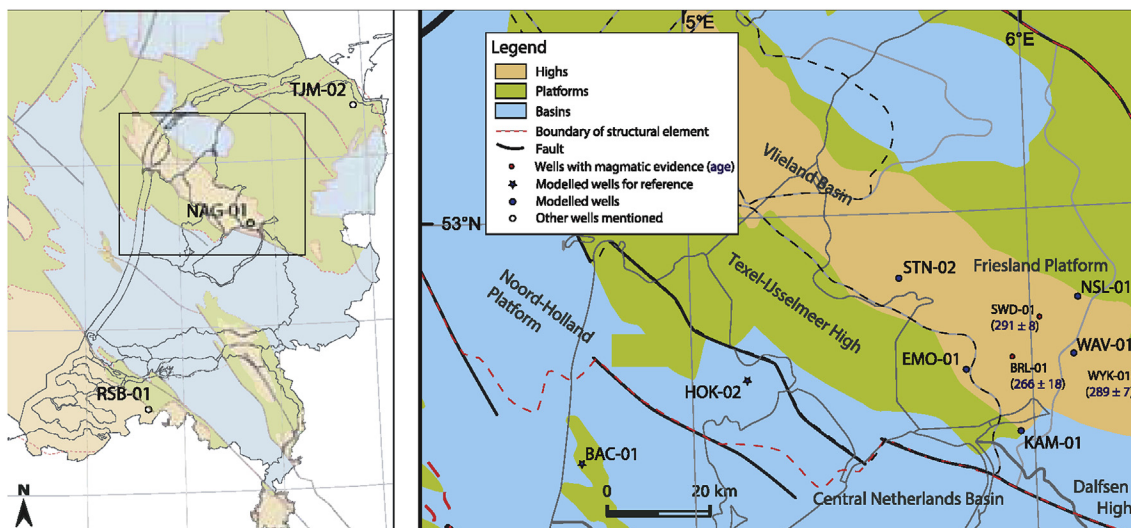


**Fig. 2.** Location of study area and wells used for the modelling. Blue dots: modelled wells. Blue stars: additional wells modelled for comparison purposes. Small red dots: wells with evidence of magmatic events during the Late Carboniferous and Permian. White dots other wells mentioned in the text. (For interpretation of the references to colour in this figure legend, the reader is referred to the Web version of this article.)

lithosphere. The sensitivities of the model parameters and evidence for the timing of the heat pulse are taken into account prior to placing the conceptual model of magmatism in the Netherlands in the broader context of North-Western Europe tectonic evolution.

Our models demonstrate that mantle upwelling and underplating at the base of the crust proposed by van Wees et al. (2000) generates insufficient heat flow to explain the strongly elevated maturity-depth trends measured between 2000 and 2500 m in the area of interest. In contrast, we propose that a widespread intrusion at shallow crustal levels provides a self-consistent mechanism for elevated heat flow with

regional impact, which explains observed high maturity-depth trends.

## 2. Geological setting and selection of the wells

### 2.1. Geological settings

The Netherlands is located on the northeastern margin of the East Avalonian micro-continent (Smit et al., 2016, 2018) and since the Late Carboniferous, the southern flank of the Southern Permian Basin (e.g. van Wees et al., 2000; Geluk, 2007a, Fig. 1; Smit et al., 2016). The
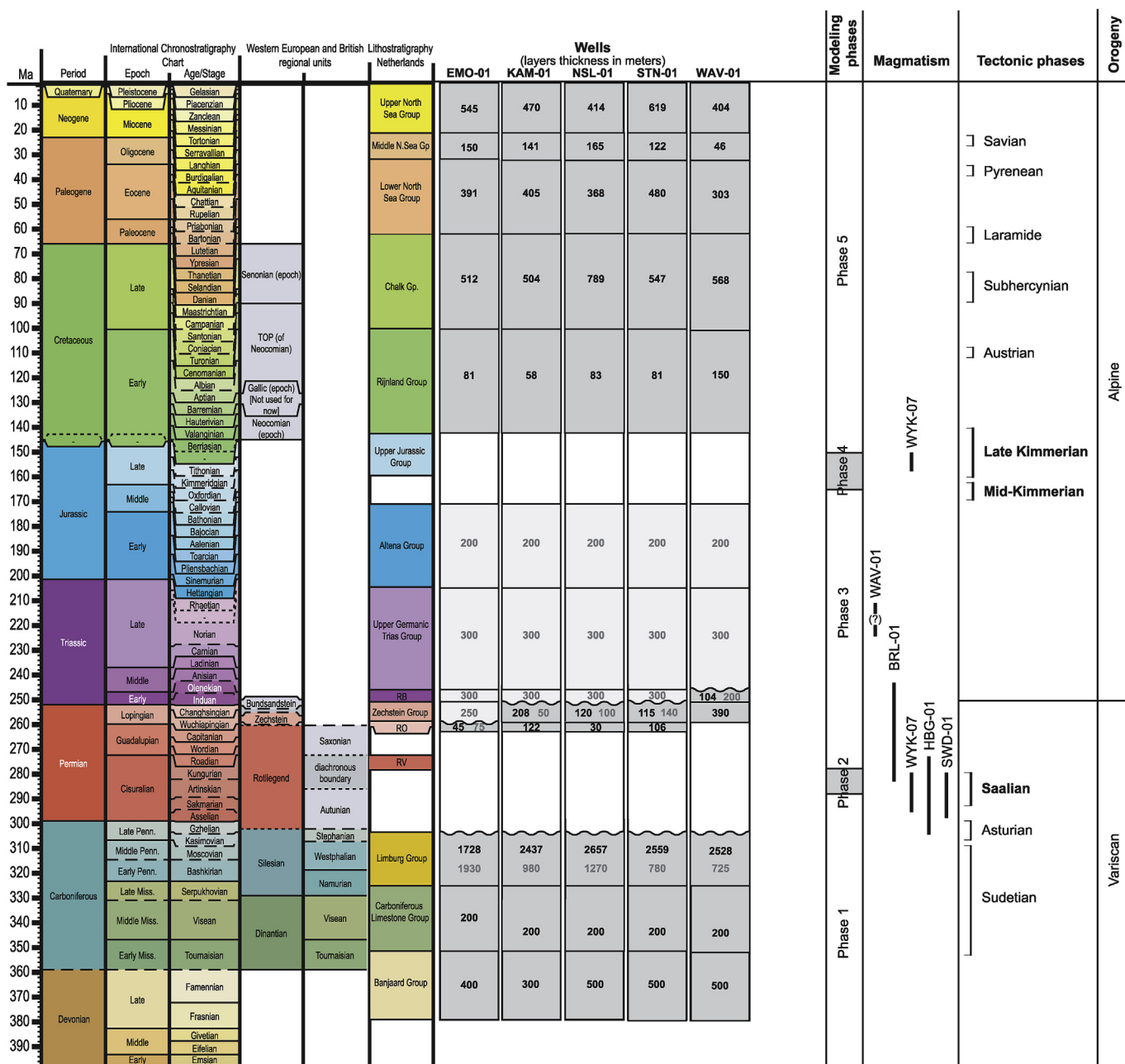
**Fig. 3.** Stratigraphic chart correlation showing lithostratigraphy of five selected wells (EMO-01: Emmeloord-01; KAM-01: Kampen-01; NSL-01: Nijensleek-01; STN-02: Sloten-02; WAV-01: Wanneperveen-01), modelled phases, magmatic evidence in the wells within the study area, and tectonic phases (from Doornenbal and Stevenson, 2010). In the well columns, the numbers correspond to the thickness of the Dutch lithostratigraphy and numbers in grey give the thickness that has been eroded while the black numbers are the thickness still present. RB: Lower Germanic Trias Group; RO: Upper Rotliegend Group; RV: Lower Rotliegend Group. The geological time scale has been made using TS-Creator that copyright of the Geologic TimeScale foundation.

tectonic and depositional evolution from the Late Carboniferous to the Lower Triassic is identical to the rest of the Southern Permian Basin, which first behaved largely as a tectonically connected structure, but this was then followed by differentiation across a number of sub-basins (e.g., Ziegler, 1990; Pharaoh et al., 2010). The focus area of this study, southwest of Texel-IJsselmeer High and southeast of the Friesland Platform (Fig. 2), has experienced multiple tectonic phases of regional compression and extension from the Carboniferous to Tertiary (e.g. Rijkers and Geluk, 1996; Smit et al., 2018).

The oldest known sediments in the Netherlands are of Late Devonian age (Geluk et al., 2007; Kombrink et al., 2008). The Devonian sediments have been drilled on very few occasions in the Netherlands and their description relies primarily on wells from neighbouring countries from which we know that they are mostly detric, siltstone and claystone with limited sandstone intervals. Devonian limestones are known from onshore Belgium and nearby Germany as well as from offshore (e.g. Geluk et al., 2007). The tectonic setting in which they were deposited remains largely unknown due to the limited number of wells and seismic data quality. Possibly, and in analogy with other parts of East Avalonia, the Netherlands were already affected by back-arc extension in the Late Devonian but this remains to be confirmed. Confirmed back-arc extension did occur in the Lower Carboniferous (Dinantian) related to slab rollback of the Rhenohercynian oceanic lithosphere that subducted northward (in today's reference frame) under Avalonia, this subduction zone was located south of the Ardennes (e.g. Smit et al., 2018). Extension formed a system of several highs, partly

covered by carbonate platforms and marine basins (e.g. Kombrink et al., 2010). At the onset of the Late Carboniferous (Silesian, Fig. 3), the Variscan orogeny led to the final amalgamation of Pangea by closure of the Rheohercynian and Rheic Ocean and attachment of the remaining peri-Gondwanan terranes to the southern margin of Laurussia, of which Avalonia was already part (e.g. Ziegler, 1990; Ballèvre et al., 2009; Nance et al., 2012). For the Netherlands, this meant the end of back arc extension. During the Late Carboniferous the Netherlands was part of the Variscan foredeep with wrench-related basins forming towards the end of the Variscan orogeny (latest Carboniferous). Tectonic accommodation space increased due to combined post-extensional thermal relaxation and foredeep flexure (Kombrink et al., 2008). As a result, the accumulated clastic deposits reached a thickness up to 4000 m, which is much thicker than any of the younger overlying units (Kombrink et al., 2008). The Silesian, Late Carboniferous, deposits are mainly detritic with depositional environments ranging from fluvial floodplains to lacustrine/marine, depending on their position in the basin. The units are primarily composed of shale in the lower part and of shale, silt, sandstone, and coal in the upper part with the coal reaching a total proportion of around 2% (van Buggenum and Den Hartog Jager, 2007). With the waning of the mantle plume and the regional igneous activity, thermal subsidence created the Southern Permian Basin during the Late Permian (Ziegler, 1990; van Wees et al., 2000). In the Netherlands, the oldest remaining Permian sediments are of Late Permian age (upper Rotliegend Group), represented by arid fluvial, aeolian and playa deposits (Gast et al., 2010). The following Zechstein Group (see Fig. 3) is dominated by evaporites of moderate thickness in the northern half of the Dutch subsurface but limited in the south. Due to its fast southward thinning out, the stratigraphy of the Zechstein shows strong lateral differences. In the south, the layers remain relatively homogenous in thickness and are only impacted by compaction, while in the north, salt flow has generated numerous pillars, salt walls, and diapirs (e.g. Geluk, 2007a). Evidence of Permian magmatism has been encountered in several Dutch wells, particularly to the east of the Texel IJsselmeer High. The extension of the magmatism remains uncertain. The Triassic to Early Jurassic sedimentation in most of the Netherlands developed under continuing thermal subsidence, leading to broad regular facies. During Middle and Late Triassic, the Early Kimmerian extension formed a number of roughly N-S oriented basins, including the North Sea Central, Horn and Glückstadt Grabens. These basins are interconnected by large wrench faults, one of them the Hantem fault along the northern margin of the Texel IJsselmeer High. Although some Triassic tectonic activity has been recorded in the Broad Fourteens and West Netherlands Basins and the Roer Valley Graben (e.g. Van Wijhe, 1987; Geluk, 2005, 2007b; Alves and Elliott, 2014; Ward et al., 2016), this early Kimmerian phase seems to have had relatively little effect on most of the Netherlands south of the Central Graben, including the Texel-IJsselmeer High (Geluk, 2005, 2007b). The main source of the Permian and Triassic clastics are the Variscan Mountains to the south. The Lower Triassic Lower Germanic Group is composed of lacustrine fine-grained siliciclastic sediments, intercalated with fluvial and aeolian sandstone (Geluk, 2005, 2007b). The Middle-Upper Permian Upper Germanic Group consist of marine to lacustrine, fine-grained siliciclastics, carbonates and evaporites. The Jurassic is a period of extension and thermal perturbation with the formation of several smaller fault-bounded basins and highs, also to the south of our study area. The Early and Middle Jurassic (Altena Group) pre-rift succession is composed of argillaceous shallow marine sediments. The Late Jurassic (Burgers and Mulder, 1991) syn-rift succession shows important spatial variations due to the newly forming sub-basins. The Early Cretaceous post-rift phase was accompanied by a large transgression across the highs in the Netherlands during the Albian. As a result, the clastic sedimentation gave way to widespread chalk and carbonate sedimentation. During the Late Cretaceous (Santonian), compressive movement resulted in the inversion of the main Jurassic rift basins and caused significant erosion (de Jager, 2007). During the Tertiary, broad upwarping of some of

these basins occurred, mostly depositing siliciclastic sequences.

Magmatism in the Netherlands is known from over sixty wells, compiled by van Bergen and Sissingh (2007). From this database, it appears that virtually all encountered igneous rocks have a mafic composition with a moderate to alkaline content, indicating mantle-derived magma with little differentiation. The evidence of magmatic activity is mostly intrusive, with the Late Jurassic Zuidwal Volcano (ca. 145Ma) as the main extrusive exception (Fig. 1). Early Devonian felsic intrusion (410 ± 7 Ma on U-Pb for the granite emplacement; Pharaoh et al., 2006), Late Carboniferous-Early Permian (~305-295 Ma) and Late Jurassic (145–160 Ma) have been identified onshore in the Netherlands. The Early Devonian granitic intrusion are emplaced in the crystalline basement on the eastern flank of the Mid North Sea High (e.g. ter Borgh et al., 2018) and further to the west in northern England (e.g. Brown et al., 2008). These so-called Newer Granites or Trans-Suture Suite post-date subduction of the Iapetus ocean, their emplacement has been attributed to different mechanisms such as transtension (e.g. Brown et al., 2008) and slab break-off (Miles et al., 2016). In contrast, later magmatic activity from the Carboniferous to the Jurassic has a more mafic composition and shows a chemical composition with an intra-plate tectonic affinity, i.e. non-oceanic or subduction-related (van Bergen and Sissingh, 2007).

The mantle plume emplacement at the Permo-Carboniferous boundary (Torsvik et al., 2008) at the early stages of the Southern Permian Basin (i.e., in the Late Carboniferous) caused magmatic underplating in the Netherlands (Ziegler et al., 2004; van Wees et al., 2000). Direct evidence of magmatism in the Netherlands during this period is limited to intrusions (with the exception of a single example of extrusive evidence in the SWD-01 well) connected to the peripheral position of the Netherlands within the Southern Permian Basin (Rijks Geologische Dienst, 1993). However, magmatism in the Southern Permian Basin during the Late Carboniferous (Fig. 1) is readily identifiable, with large extrusive deposits in Germany and the Central Graben, as well as intrusive rocks in Germany, northern Denmark and the Oslo Graben (Heeremans et al., 2004; Torsvik et al., 2008). The Jurassic North Sea rifting had a strong influence on the sedimentation. Rifting was accompanied by some magmatic activity. In the Netherlands, much of the evidence is intrusive, located within the West Netherlands Basin and the Broad Fourteens Basin (e.g. Ziegler, 1990; Wong, 2007). Fluid and gas escape features such as the gas pipes in the Upper Jurassic of the Broad Fourteens Basin could be related to magmatic activity as well. However, as convincingly argued by Ward et al. (2016), these Late Jurassic fluid escape features can be related to high overpressures due to abnormally high sedimentation rates. This explanation is supported by the termination of the most recent gas pipes at the Jurassic-Cretaceous boundary, which coincides with the end of Late Jurassic high sedimentation rates Ward et al. (2016).

## 2.2. Well selection

We have selected the vicinity of the Texel IJsselmeer High and Friesland Platform (Fig. 2) as our study area for the heat flow in the Southern Permian Basin. This area has been selected for three main reasons. Firstly, the layers older than Jurassic age, have never undergone a higher grade thermal influence (neither increased heat flow and eroded volume) relative to the Permian event. Consequently, the Carboniferous maturation in this area has not been overprinted compared to basins that have experienced deep burial and inversion after the latest Carboniferous-Permian (e.g., van Balen et al., 2000; de Jager, 2007). Secondly, a large number of wells have been drilled into the thick Carboniferous section (Kombrink et al., 2008). Thirdly, many wells in this area show evidence of magmatic activity at the very end of the Carboniferous and Permian and in the nearby Lower Saxony Basin (Fig. 1). No evidence of Cretaceous magmatism has been recorded on the Texel-IJsselmeer High, the youngest recording intrusion dates from the Early Jurassic. At the Late Jurassic, the Zuidwal volcano was active
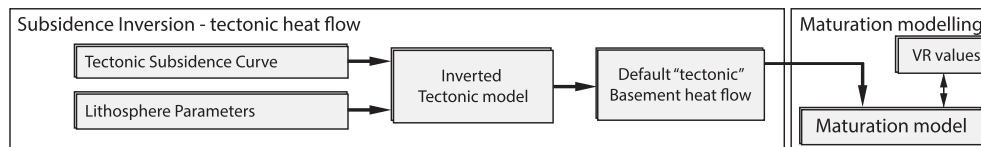
**Fig. 4.** General workflow adopted in the modelling approach (modified after van Wees et al., 2009). VR values: Vitrinite Reflectance values.

north of the Texel-IJsselmeer.

The five selected wells (Figs. 2 and 3) were chosen for their good representation of the area of interest, as well as for their abundance of maturity data. Wanneperveen-1 (WAV-01) is a "wildcat" gas exploration well and reached 2070 m in 1951. Emmeloord-1 (EMO-1) was drilled in 1968-69 to a depth of 2547 m. Kampen-1 (KAM-01) was initially drilled in 1969 to 1569 m, and deepened later to 2154 m. Sloten-2 (STN-2) is an exploration well that was drilled in 1982–2547 m total depth. Nijensleek-1 (NSL-01) was drilled in 1987 to a total depth of 2327 m. In addition; Bakkum-Castrium-01 (BAC-01) and Hoogkarspel-02 (HOK-02) that respectively reached a depth of 2282.5 m and 2061.2 m will be modelled to assess the correlation between the maturation of the five wells mentioned above and the intrusion.

The sediment descriptions of the wells have been extracted from the lithostratigraphic description available on the nlog website (www.nlog.nl) (Fig. 3). The recorded depth has been corrected from the deviation of the wells. However, none of these wells reached the depth of the basement. According to Geluk (2007a), the top of the Silurian basement is at a depth of less than 5000 m in the selected area. Following the information available from Wong et al. (2007), van Adrichem Boogaert and Kouwe (1997), and the newly drilled well Luttelgeest-1 (which reached the Dinantian), we have been able to extrapolate the missing deeper sections.

### 2.3. Tectonic evidence

The wells are marked by two main erosion phases (Fig. 3). The first phase, of Upper Carboniferous-Early Permian age, occurs from 290 to 280 Ma (Gradstein et al., 2004). The lithology of the rock system in which is the geochemical record of the first erosional phase, correspond to a monotonous succession of fine-grained siliciclastic sediments. This mega-unconformity has been referred to as the "Base Permian Unconformity" (Geluk, 2005). Erosion affected strata of Upper Carboniferous to Permian-age according to the "Western Europe" Geological Time Scale (Ogg et al., 2008). The eroded strata mainly consist of latest Carboniferous units (Limburg Group), with the exception of the well Emmeloord-1, where the erosion has reached deeper levels. The estimated eroded thicknesses are based on isopach maps of the latest Carboniferous stages (van Buggenum and Den Hartog Jager, 2007). In total, the total thickness eroded during this phase is between 725 m (Wanneperveen-1) and 1930m (Emmeloord-1). These differences can be explained by a folding event, which was created by the transpressional movement that culminated during latest stages of the Variscan orogeny (van Buggenum and Den Hartog Jager, 2007).

The second erosion phase, during the Kimmerian tectonic phase, is an amalgamation of several pulses from Mid-to Late Jurassic described in detail in Wong (2007) and Herngreen and Wong (2007). The uplift that can be related to the Arctic-Atlantic-North Sea rifting (Ziegler, 1990) exposed our study area to sub-aerial erosion (Wong, 2007) during the Upper Jurassic (154.5–147.5 Ma) in conjunction with rifting and sedimentation in the surrounding basins. The period of erosion lasted 14My (from 164 Ma to 150 Ma) on the southern Texel-IJsselmeer High (Wong et al., 2007; Van Adrichem Boogaert and Kouwe, 1997). The erosion affected the following layers (Wong et al., 2007): the Slochteren Formation (ROSL, Mid-Permian), the Zechstein Group (ZE, Late Permian), the Lower Germanic Trias Group (RB, Late Permian to Early Triassic), the Upper Germanic Trias Group (RN, Early Triassic to Late Triassic), and the Altena Group (AT, Late Triassic to early Late Jurassic).

For the wells Kampen-1, Nijensleek-1, and Sloten-2, the erosion terminated in the Late Permian. The well Wanneperveen-1 was subject to less erosion (700 m in total), with the Permo-Triassic layers being partially eroded, and the well Emmeloord-1 has experienced the largest amount of erosion (1125 m). The amount of erosion has been estimated through geometric extrapolation (cf. Pluymaekers et al., 2012) based on the nearby complete stratigraphic sections on the Friesland Platform. There are no relevant vitrinite reflectance data to constrain erosion in this area.

### 3. Methodology

The success of inversion of subsidence curves for kinematic tectonic interpretation has been demonstrated by several authors (e.g., White, 1993; van Wees et al., 1996; van Wees and Beekman, 2000; Bellingham and White, 2000). The methodology has recently been used to determine the heat flow and maturation of various basin settings (van Wees et al., 2009; Hirsch et al., 2010). The general workflow for the modelling technique is shown in Fig. 4. In the first step, a backstripping analysis is performed, resulting in a tectonic subsidence curve for each well. A tectonic modelling inversion procedure at lithospheric scale is then carried out in order to obtain the tectonic model that fits the back stripped tectonic subsidence curve. The forward modelling approach is founded on the pure-shear lithosphere thinning model of McKenzie (1978) with the possibility of different amounts of thinning in the crustal and lithospheric mantle (Royden and Keen, 1980). The stretching model allows for underplating and intrusion in the crust (Hirsch et al., 2010; Beglinger et al., 2012).

The validation of the basement heat flow is made by maturation modelling and subsequent calibration to measured maturity (e.g. vitrinite reflectance (%VR)) and present day temperature data in the wells.

Thermal boundary conditions are defined at the top of the sediments and the base of the lithosphere. The lower boundary has been set in relation to a well-known thermal limit (i.e., 1330 °C for the base of the lithosphere). The upper boundary is set based on the Sediment Water Interface Temperature (SWIT), which is a function of the Paleo-Water Depth (PWD) and which has been generated using the integrated PetroMod® tool from Schlumberger. This has been implemented in line with the study carried out by Wygrala (1989) in Northern Europe at 52° latitude north, and corrected for Late Quaternary temperature interpretation (Bonté et al., 2012) (Fig. 5).

The thermal parameters used for the lithosphere (Table 1) have been adopted from van Wees et al. (2009). A lithospheric thickness of 100 km, has been used based on Artemieva and Mooney (2001), for a specific fit with our area of interest.

For the backstripping and modelling of the temperature in the sediments, the lithology of each layer is described as a fraction of eight basic lithologies (sandstone, shale, siltstone, limestone, salt, coal, anhydrite, and dolomite). The basic lithologies have specific compaction and thermal parameters. The compaction is given by a double exponential porosity-depth law (Bond and Kominz, 1984), which is here represented by equations (1) and (2):

$$\phi(z)|_{z \Leftarrow zscalechange} = \phi_0 e^{-\frac{z}{scale}} \tag{1}$$

$$\phi(z)|_{z > zscalechange} = \left[ \phi_0 \frac{e^{\frac{zscalechange}{zscale}}}{e^{\frac{zscalechange}{zscale2}}} \right] e^{-\frac{z}{scale}} \tag{2}$$
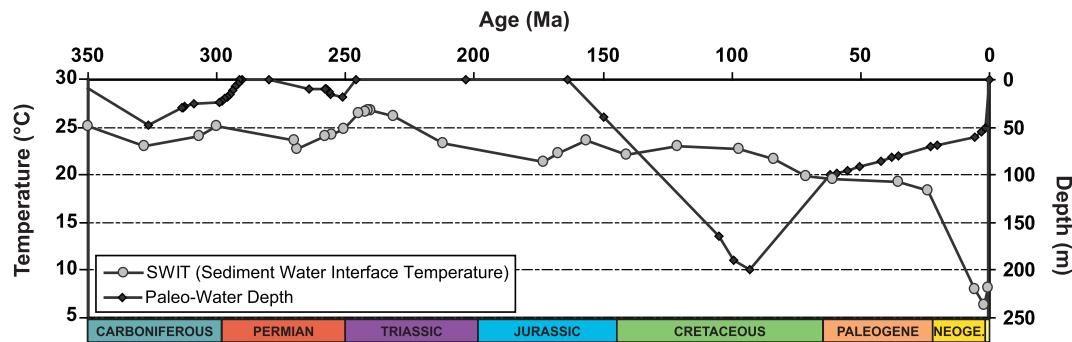
**Fig. 5.** Evolution of the paleo-water depth and Sediment Water Interface Temperature (SWIT) through time on the Friesland Platform.

**Table 1**
Thermal and geometrical parameters of lithosphere stretching model.

| Parameter | Description | Unit | Value |
|---|---|---|---|
| Lith | Lithospheric thickness | [km] | 120 |
| Crust0 | Crustal thickness | [km] | 30 |
| $\rho_{crust}$ | Crustal surface density | [kg/m$^3$] | 2900 |
| $\rho_{mantle}$ | Mantle surface density | [kg/m$^3$] | 3400 |
| $k_{crust}$ | Crustal conductivity | [Wm$^{-1}$ C$^{-1}$] | 2.6 |
| $k_{mantle}$ | Mantle conductivity | [Wm$^{-1}$ C$^{-1}$] | 3 |
| $k_{sed}$ | Bulk sediment conductivity | [Wm$^{-1}$ C$^{-1}$] | 2 |
| $A_{uc}$ | Heat production in upper crust | [mW/m$^3$] | variable |
| $A_{lc}$ | Heat production in lower crust | [mW/m$^3$] | 0.5 |
| $\alpha$ | Lithosphere thermal expansion | [-] | $3.2 \times 10^{-5}$ |
| $\kappa$ | Thermal diffusion | [m/s$^2$] | $1 \times 10^{-6}$ |
| $T_{surf}$ | Surface temperature | [C] | 20 |
| $T_{base}$ | Base lithosphere temperature | [C] | 1330 |

**Table 2**
Parameters for each lithology (source: van Wees et al., 2009). a-parameters for porosity evolution with depth where φ is porosity, z is depth (m), $\varphi_0$ is surface porosity, zscale change is depth at which porosity–depth trend changes and zscale and zscale 2 are coefficient rates; b-thermal parameters for each lithology.

a

| Lithology | $\varphi_0$ | $\varphi_{SD}$ | zscale | zscale SD | zscalechange | zscale2 |
|---|---|---|---|---|---|---|
| Sandstone | 30 | 0 | 2022 | 667 | 1000 | 3356 |
| Shale | 61.5 | 0 | 930 | 16 | 500 | 2116 |
| Siltstone | 42.5 | 0 | 2038 | 621 | 500 | 2871 |
| Limestone | 49 | 0 | 1238 | 377 | 500 | 1993 |
| Salt | 6 | 0 | 7000 | 0 | 20000 | 5000 |
| Coal | 6 | 0 | 7000 | 0 | 20000 | 5000 |
| Anhydrite | 6 | 0 | 7000 | 0 | 20000 | 5000 |
| Carbonate | 49 | 0 | 1238 | 377 | 500 | 1993 |

b

| Lithology | Conductivity (W/(m.K)) | Heat production (µW/m$^3$) |
|---|---|---|
| sandstone | 3.5 | 5.00 10$^{-07}$ |
| shale | 1.9 | 1.00 10$^{-06}$ |
| siltstone | 2.75 | 5.00 10$^{-07}$ |
| limestone | 3 | 2.00 10$^{-07}$ |
| salt | 5.5 | 0 |
| coal | 0.5 | 0 |
| anhydrite | 5.8 | 0 |
| dolomite | 3.3 | 5.00 10$^{-07}$ |
| water | 0.6 | 0 |
| HC | 0.5 | 0 |

Where z is the depth in meters, $\phi(z)$ is the porosity at the depth z, $\phi_0$ the surface porosity, and zscalechange is the depth at which the porosity-depth trend changes. The parameters for the porosity-depth curve and for each basic lithology are summarised in Table 2a. The thermal parameters, thermal conductivity (in W/m/K), and radiogenic heat

production (µW/m$^3$), are listed in Table 2b.

To invert the backstripped tectonic subsidence curve, a best-fit iterative method is used, which correlates the modelled to the observed tectonic subsidence curve. The forward modelling technique that is used to obtain the best-fitting subsidence curve is related to the stretching factors in the lithosphere and the mode of iteration. The fit is obtained in subsequent phases that correspond to tectonic stages constrained by the geological record of the area (cf. van Wees et al., 1996). The stretching factors, respectively δ and β for crustal and subcrustal stretching, can either be uniform (i.e., δ = β; McKenzie, 1978) or two-layered (i.e., δ ≠ β; e.g., Royden and Keen, 1980). In order to generate the most accurate best-fit, the sedimentation history has to be split into phases. The stretching factors can be selected as (partially) fixed. Following van Wees et al. (2000, 2009), magmatic events are modelled with a fixed β≫1 condition to reproduce the effect of mantle upwelling and thermal uplift. An important consequence of lithospheric thinning is the change in pressure that occurs adiabatically, resulting in the partial melting of harzburgites and other mantle rocks. As these melts migrate upwards, they can mix with crustal rocks and either extrude or become trapped into the lower crust as massive underplated bodies of a specific thickness (e.g. White et al., 2018; François et al., 2018).

## 4. Results and discussion

### 4.1. Backstripping and tectonic modelling

The results of the backstripped tectonic subsidence and best-fit tectonic subsidence reconstruction from forward modelling (use of physical equations to model parameters for a given geological situation) of the five modelled wells are presented in Fig. 6. The result of the tectonic heat flow modelling is a basement heat flow (HF) curve for each of the wells (Fig. 7). The record in the sedimentation and the determined erosional phases highlight five key phases, which have been adopted in the forward model. These model phases and used iteration modes are listed in Table 3 and described in detail below.

Phase 1 is related to initial sedimentation linked to early Variscan extension. The increase of accommodation space for sedimentation from 326 Ma onwards is connected to the onset of Variscan compression, which led to the formation of a foreland basin. Phase 2 is marked by post-Variscan uplift. Following the Early Permian thermal perturbation related to mantle plume emplacement (cf. Ziegler et al., 2004), Phase 3 is characterised by an increase in basin subsidence due to thermal relaxation. During the Middle and Upper Jurassic, the North Sea Rift is affected by doming creating some uplift in our study area (Phase 4). In Phase 5, sedimentation becomes predominant after the cessation of North Sea rifting.

The first phase (374.5–294 Ma) extends from the origin of the basin during the Devonian to the end of the Carboniferous at 294 Ma. This phase (Table 3) is modelled with a "bdcoup" iteration mode, representing a uniform lithospheric stretching model (cf. McKenzie, 1978). The basin formation started in response to the back arc
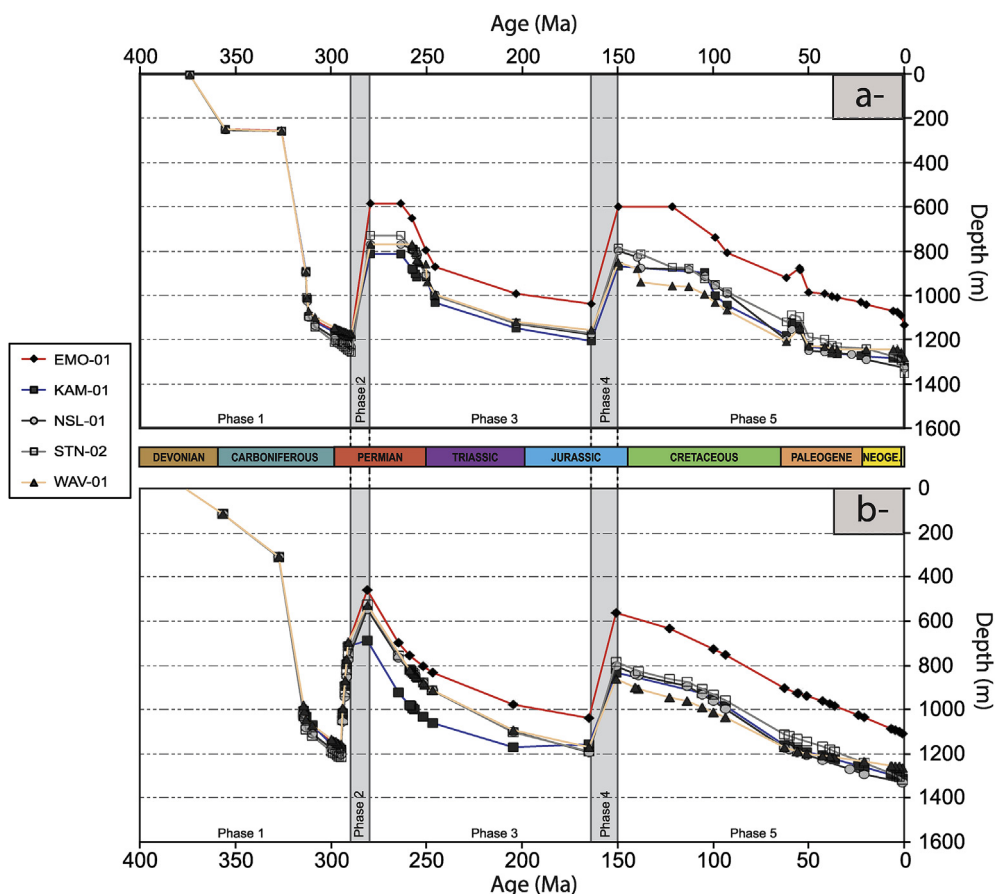
**Fig. 6.** Tectonic subsidence of five modelled wells and phases for the models. a- Observed tectonic subsidence. b- Modelled tectonic subsidence.

extension to the SE of the Netherlands during the Devonian (Allen and Allen, 2005). During the Late Carboniferous, closure of the Rheic Ocean and the loading of the lithosphere by Variscan thrust sheets led to the development of the Silesian foreland basin. Increased topography and erosion of the nearby Variscan mountain chain result in an increased sedimentation rate (Ziegler, 1990). The rise of sea level in the Early Silesian (Ross and Ross, 1987) should also be taken into account in connection with the increase in sedimentation rates at that time. The Early and Middle Silesian deposition are deposited in relatively low-energy marine environments (Geluk et al., 2007). The following

deposits dated Late Silesian, mark a slowing down in sedimentation rates in connection with the cessation of Variscan convergence. As a result of a decrease in tectonic subsidence, the available accommodation space decreased and the depositional environment became more continental with coastal swamp or fluviatile depositional environments (van Buggenum and Den Hartog Jager, 2007).

The second phase corresponds to the "Saalian" erosive uplift tectonic phase (294-280 Ma), which is part of the more widely recognised Base Permian Unconformity that spans from 315 to 265 Ma (Pharaoh et al., 2010). This phase is connected to the cessation of convergence
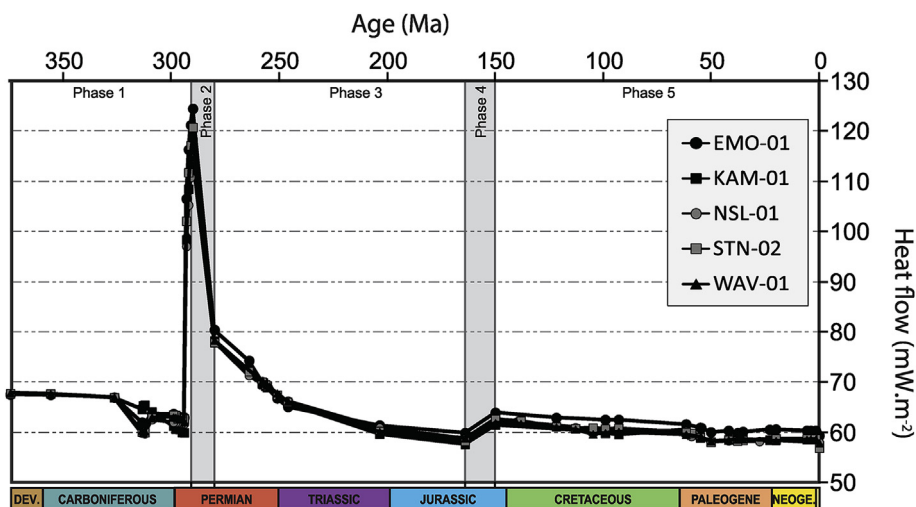


**Fig. 7.** Basement heat flow of five modelled wells.

**Table 3**
Phases used for modelling of five wells (see van Wees et al. (2009) for details). δini: initial stretching factor for the crust, βini: initial stretching factor for the lithospheric mantle. For iteration methods: "bdcoup" refers to a coupled stretching method (McKenzie, 1978), while "bdfixed", and "dfree" refer to a de-coupled stretching method (Royden and Keen, 1980). For the depth of the intrusion, 1 refers to the base of the lithosphere and refers to the top of the upper crust (i.e. the top of the basement).

| Phase # | Phases | | | | | Intrusion | | |
|---------|--------|---|---|---|---|-----------|---|---|
| | Phase start (Ma) | Phase end (Ma) | Iteration mode | $\beta_{ini}$ | $\delta_{ini}$ | thickness (m) | temperature (°C) | depth |
| Phase 5 | 150 | 0 | bdcoup | 1 | 1 | 0 | 0 | 1 |
| Phase 4 | 164 | 150 | dfree | 1.2 | 1 | 0 | 0 | 1 |
| Phase 3 | 280 | 164 | bdcoup | 1 | 1 | 0 | 0 | 1 |
| Phase 2b | 290 | 280 | dfree | 1.3 | 1 | 0 | 0 | 1 |
| Phase 2a | 294 | 290 | bdfixed | 2.5 | 1.15 | 4000 | 1100 | 0 |
| Phase 1 | 374.5 | 294 | bdcoup | 1 | 1 | 0 | 0 | 1 |

(Rijks Geologische Dienst, 1993) and pervasive Permo-Carboniferous plume-related magmatism (van Bergen and Sissingh, 2007; Torsvik et al., 2008). In order to reproduce a pervasive magmatic influence on modelled heat flow and elevated maturation depth trends in the Carboniferous section, we separate the uplift phase into two distinct sub-events in the model. These consist of a magmatic intrusion (phase 2a) associated with considerable mantle attenuation, followed by crustal attenuation and erosion (phase 2b). Please note that by increase of mantle attenuation (although in 1D model) will increase the heat flow (Carboniferous) across the entire basin area. Such inversion will not fully replace limited affection of magmatic intrusions in two- or three-dimension numerical space. For the magmatic intrusion event, sub-crustal and crustal stretching values have been set to 2.5 (cf. van Wees et al., 2000) and 1.15 respectively. The crustal stretching value of 1.15 compensates for thermal and underplating uplift in line with the observed tectonic subsidence evolution. The magmatic intrusion is assumed to be 4000 m thick, and is positioned only shallowly in the crust at the base of the sediments, at an emplacement temperature of 1100 °C. The end of this event is marked by a peak in both heat flow and temperatures in the Carboniferous section at 290 Ma, just prior to the major Saalian erosion (Fig. 7). The comparison between the modelled tectonic subsidence (Fig. 6b) and the observed tectonic subsidence (Fig. 6a) illustrates the effect of the intrusion, which creates an uplift of the basement before the extension event.

The second sub-event of this phase reflects the lateral spreading of the plume-head in later stages of its existence (e.g. François et al., 2018). Within the model, this erosive phase is marked by a slight crustal attenuation and more pervasive mantle attenuation that reflects the thermal effects of hot mantle material replacing the relatively cold mantle (van Wees et al., 2000). The result of this sub-phase is a prolonged uplift in the tectonic subsidence curve (Fig. 6b) between 290 Ma and 280 Ma. This main uplift in phase 2a appears to have shifted to the main uplift that was suggested in the backstripped tectonic subsidence curve of phase 2b. This shift can be explained by an increase in paleo-topography in the period from 294 to 290 Ma, and its waning in the period from 290 to 280 Ma. It is only through such an interpretation of paleo-topographical evolution that the model is capable of reaching a heat flow peak in maximum sediment burial during uplift in the Carboniferous.

The third phase (280–164 Ma) reflects the thermal sag of the Southern Permian basin (Cloetingh and Ziegler, 2007) following the Permo-Carboniferous heat pulse, enhanced by intermittent and moderate local lithospheric thinning. The model adopts a "bdcoup" iteration mode in order to allow the model to fit the data. The sedimentation record is marked by a depositional hiatus, which started after the uplift and erosion of the previous phase (280 Ma) and lasted until 264 Ma, with the Mid-Permian, the first to be deposited, characterised by continental depositional environments (i.e., fluvial systems separated by eolian deposits; Geluk, 2007a). The modelled tectonic subsidence curve appears to produce the thermal sag more rapidly than the observed

backstripped tectonic subsidence. As pointed out by van Wees et al. (2000), this discrepancy is consistent with the thermal subsidence of the Southern Permian Basin below global sea level.

In the Lower Triassic there is a degree of differential subsidence, whereas the Upper Triassic is considered as a post-rift event (Geluk, 2007b). The thickness of the depositions, not uniform in the Netherlands, is estimated to be around 600 m in our area of interest. The sea progressively deepens in the Lower and Middle Jurassic, creating pronounced depositional thickness variations (i.e., ranging between a few metres and 1800 m; Wong et al., 2007), 200 m in our area. According to the tectonic subsidence curve, these depositional stages can be considered as post-rift (Fig. 6), consistent with findings by Geluk (2007b). However, it appears from the differentiation in the sedimentation that some extended tectonics still has some effect (Wong et al., 2007). From the Aalenian onward, the North Sea Rift started to develop in the northern parts of the North Sea (Underhill and Partington, 1993). The effect of this uplift shifted south and became effective in the Netherlands during the Oxfordian (i.e., around 164 Ma ago).

During the last stage of the Jurassic (late Oxfordian to Kimmeridgian), the uplift in the North Sea affected the Dutch onshore, causing deep erosion into the older layers (e.g. Ziegler, 1990; Underhill and Partington, 1993; Wong, 2007). We model the phase 4 of this period (164-50 Ma) with a fixed stretching factor of 1.2 for the lithospheric mantle. With this method, we describe a rifting phase with mantle heating and magmatism (van Wees, 2007; van Wees et al., 2000). The magmatism in the Dutch onshore was more local and less intense than the Permo-Carboniferous plume-related magmatism, in conjunction with the location of the Netherlands at the southern border of the area affected by rifting and magmatism (e.g. van Bergen and Sissingh, 2007). Geographically, the major Jurassic magmatism is centred between Scotland and Norway (Ziegler, 1990; van Bergen and Sissingh, 2007). In our study area, only the well Baarlo-1 shows some evidence of magmatic intrusions (van Bergen and Sissingh, 2007). Layer-wise, the Altena Group (Lower Jurassic) and the Upper Germanic Trias Group (Middle to Upper Triassic) have been eroded in all the wells at this stage. In the well Wanneperveen-1, which shows the least erosion, the Lower Germanic Trias Group is only partly eroded, while for the wells Kampen-1, Nijensleek-1, and Sloten-2, the erosion cuts into in the Zechstein Group. For well Emmeloord-1, which shows the highest erosion, the erosion reaches the Upper Rotliegend Group. At the scale of our study area, the original thickness of the deposits from the Permian (i.e., Upper Rotliegend Group) to the Lower to Middle Jurassic (i.e., the Altena Group) were laterally constant.

In the last stage (150-0 Ma), phase 5, sedimentation is predominant. In order to model this event, we use a "bdcoup" iteration method with a start beta and delta of 1. However, as the observed tectonic subsidence (Fig. 6a) shows a minor uplift peak at the Cretaceous-Tertiary Boundary, the model takes into account two different phases. The first phase covers the Cretaceous, which includes the Rijnland Group (Early Cretaceous) and the Chalk Group (Late Cretaceous). The second phase

covers the Tertiary, comprising the Lower North Sea Group (Palaeocene and Eocene), the Middle North Sea Group (Oligocene), and the Upper North Sea Group (Neogene and Quaternary).

The Cretaceous sedimentation builds up gradually from north to south. The sedimentation of the Early Cretaceous Rijnland Group begins at 140 Ma for the Sloten-2 and Nijnleek-1 wells, while it starts at 104.8 Ma for the Kampen-1 well. This time-lag for the onset of sedimentation is connected to the transgression, which takes time to develop between the Friesland Platform and the Texel Ijsselmeer High (Herngreen and Wong, 2007). The deposition of the Chalk Group (Late Cretaceous) marks a change in the sedimentation: during the Albian the highs were progressively flooded (Crittenden, 1987) allowing more carbonate sedimentation. The early deposition of the Chalk Group is, like the Rijnland Group, in a post-rift setting but from the Santonian onward compressive forces related to the onset of the Alpine collision result in the inversion and of all major Late Jurassic basins. This Alpine phase, called the Subhercynian inversion, caused important erosion in the Jurassic basins but had limited to no effect on the uplift of the Texel IJsselmeer High/Friesland Platform. The sedimentation in this study area slowed down without indications of erosion. The deceleration of the sedimentation and the absence of erosion in the layers explain the lack of any peak in the measured tectonic subsidence curve (Fig. 6b). The Tertiary succession that followed this last rebound has a thickness of around 1000 m, with some slight differences across our study area.

### 4.2. Maturation modelling

In order to test if observed VR values are corresponding to our model, we predicted maturity using the Easy%Ro kinetic model of Sweeney and Burnham (1990), based on a time-variable temperature gradient in the basin sediments, in agreement with the calculated tectonic basement heat flow (cf. van Wees et al., 2009), and taking into account the effects of depth-dependent porosities in the basin sediments and related changes in thermal conductivity (cf. Table 1).

The result of the maturation modelling is a maturation gradient for five of the wells discussed here. This gradient is then compared to the measured values available in each of the considered wells and summarised in Table 4. The observed values are an average of the measurements in a given well at a certain depth, the reliability of the value is given by the standard deviation of the vitrinite reflectance, which is related to the variation of the data encountered. The quality of the measurements is rather good marked by standard deviations of

0.04–0.37, with an average of 0.10.

The results of the maturation modelling for the five selected wells (Fig. 8) show a good correlation between the model and the measured values. Only the wells Nijensleek-1 and Wanneperveen-1 slightly overestimate the vitrinite reflectance value in comparison to the measurements. The wells can be divided into different categories based on their geographical position from the major structures in the area. The Emmeloord-1 well, located in the Texel IJsselmeer High, has the highest VR increase with depth as the thermal modelling reaches a maximum of the maturation value of 4.66% (maximum limit of the EasyRO% algorithm) at 4352 m (Fig. 8a). This high value can be explained with the tectonic subsidence curve (Fig. 6), which we interpret as having a stronger erosion and precursor subsidence. The organic matter in this well is therefore subjected to a significantly higher maximum temperature than that in the Kampen-1 well, which has a low VR increase with depth (Fig. 8b), having remained closer to the surface at time of the heat flow peak. In addition, the thermal impact of the intrusion on the maturation is also reduced by a sediment thickness in excess of the Emmeloord-1 well. The remaining wells (Sloten-2, Nijensleek-1, and Wanneperveen-1) are located in the southern part of the Friesland Platform. For these three wells, both the observed and modelled curves for the tectonic subsidence (Fig. 6), as well as the basement heat flow curves (Fig. 7), show similar patterns. The VR curve of Sloten-2 (Fig. 8d) has a lower gradient then Nijensleek-1 and Wanneperveen-1 (Fig. 8c and e), but the calculated VR curves of Nijensleek-1 and Wanneperveen-1 are overestimated in terms of the VR values available. This can be explained by a slightly lower erosion during the Early Permian compared to the Sloten-2 well. As a confirmation, we also obtained information for the VR reflectance values for the following wells (Fig. 2) Nagele-01 (NAG-01), Tjuchem-02 (TJM-02), and Rijsbergen-01 (RSB-01). These 3 wells show VR values above 5% for the Epen Fm (Namurian), which confirm the high heat flow.

Geologically, the two main parameters, which are likely to influence the VR anomalies in the study area, are the excess burial related to hiatuses in the stratigraphic record and the elevated thermal gradient through the increase of heat flow at the base of the model. The erosion phases are considered to be well-constrained as a result of the maximum reconstructed thickness approximations from wells and seismic data (Geluk, 2007b). As a result, the uncertainty is solely due to the basement heat flow, with main variations largely caused by the intrusion at the latest Carboniferous-Permian (i.e., Phase 2a). The main parameters from the intrusion influencing the heat flow are position in

**Table 4**
Vitrinite reflectance values of five analysed wells. VR stands for vitrinite reflectance, SD for standard deviation, N for the number of measurements, and T for vitrinite reflectance (Rr: mean vitrinite reflectance; Rmax: maximum vitrinite reflectance).

| Well | Depth (m) | VR (%) | VR SD (%) | VR min (%) | VR max (%) | Cuttings/Core | N | T | Formation name | Age | Lithology |
|---|---|---|---|---|---|---|---|---|---|---|---|
| EMO-01 | 1784.00 | 0.92 | 0.06 | | | Cuttings | 50 | Rmax | Baarlo Fm. | Carboniferous | Shaly sandstone |
| EMO-01 | 1846.00 | 0.89 | 0.05 | | | Cuttings | | Rr | Baarlo Fm. | Carboniferous | Shaly sandstone |
| EMO-01 | 2002.00 | 1.08 | 0.05 | | | Cuttings | 50 | Rmax | Epen Fm. | Carboniferous | Sandstone and silt |
| EMO-01 | 2434.45 | 1.88 | 0.37 | | | Core | 5 | Rr | Epen Fm. | Carboniferous | Sandstone and silt |
| EMO-01 | 2546.60 | 2.13 | 0.25 | | | Core | 28 | Rmax | Epen Fm. | Carboniferous | Sandstone and silt |
| KAM-01 | 1941.00 | 0.63 | | 0.17 | 0.24 | Cuttings | | Rr | Ruurlo Fm. | Carboniferous | Shaly sandstone |
| KAM-01 | 2025.00 | 0.87 | | 0.26 | 0.31 | Cuttings | | Rr | Ruurlo Fm. | Carboniferous | Shaly sandstone |
| KAM-01 | 2130.00 | 0.72 | | 0.21 | 0.25 | Cuttings | | Rr | Ruurlo Fm. | Carboniferous | Shaly sandstone |
| NSL-01 | 2322.00 | 0.79 | 0.06 | | | Core | 50 | Rr | Baarlo Fm. | Carboniferous | Shaly sandstone |
| NSL-01 | 2250.00 | 0.71 | 0.05 | | | Cuttings | 49 | Rr | Baarlo Fm. | Carboniferous | Shaly sandstone |
| NSL-01 | 2280.00 | 0.71 | 0.06 | | | Cuttings | 50 | Rr | Baarlo Fm. | Carboniferous | Shaly sandstone |
| NSL-01 | 2310.00 | 0.83 | 0.07 | | | Cuttings | 50 | Rr | Baarlo Fm. | Carboniferous | Shaly sandstone |
| STN-02 | 2150.00 | 0.64 | | | | Core | | Rr | Ruurlo Fm. | Carboniferous | Shaly sandstone |
| STN-02 | 2210.00 | 0.63 | | | | Cuttings | | Rr | Baarlo Fm. | Carboniferous | Shaly sandstone |
| STN-02 | 2210.00 | 0.64 | 0.04 | | | Cuttings | 50 | Rr | Baarlo Fm. | Carboniferous | Shaly sandstone |
| STN-02 | 2235.00 | 0.58 | 0.04 | | | Cuttings | 50 | Rr | Baarlo Fm. | Carboniferous | Shaly sandstone |
| WAV-01 | 1990.00 | 0.38 | 0.05 | | | Cuttings | 50 | Rr | Ruurlo Fm. | Carboniferous | Shaly sandstone |

## Vitrinite reflectance (%)
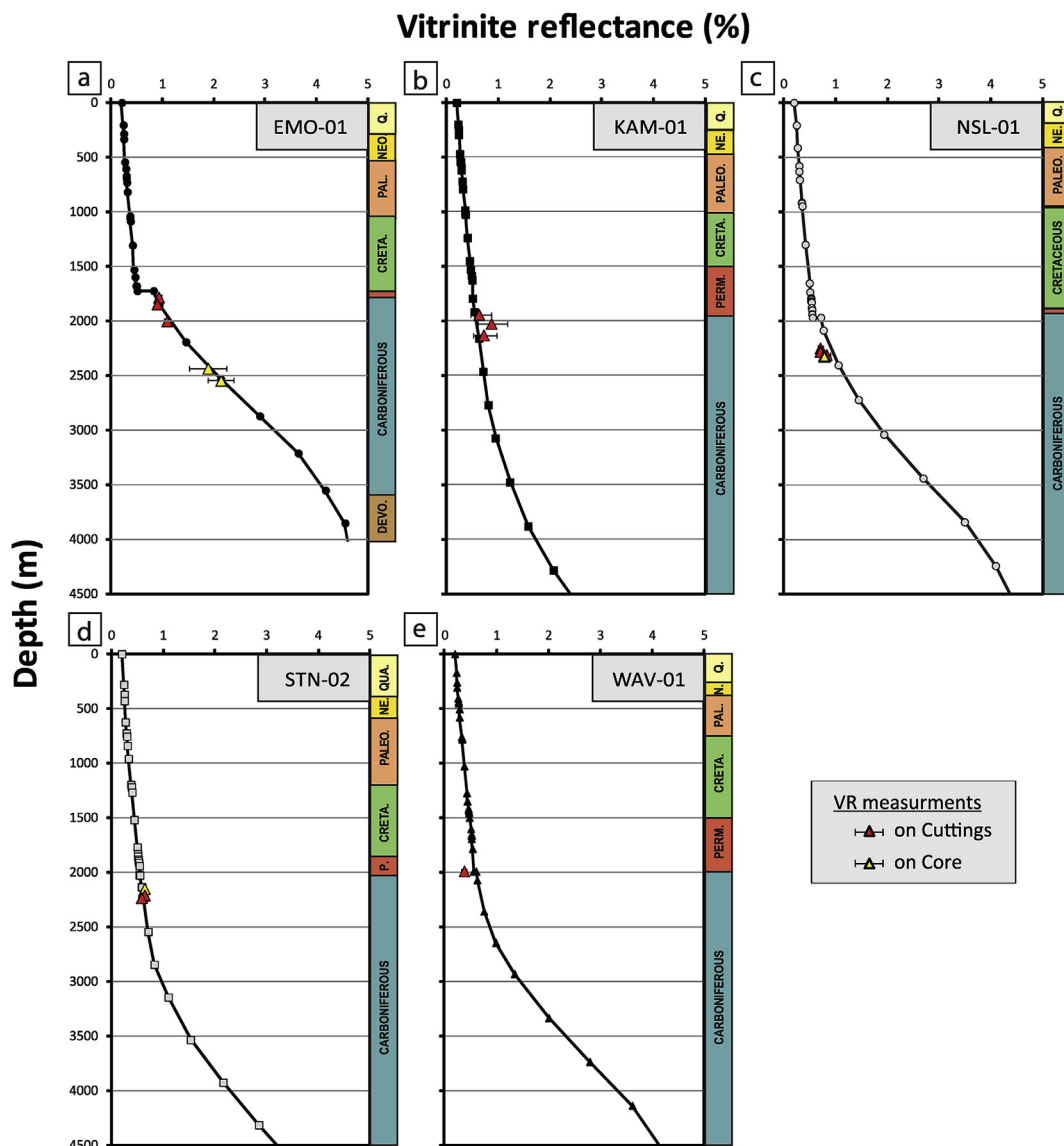


**Fig. 8.** Results from vitrinite reflectance modelling. Modelling results are compared to measured values (red triangle for the measurements on cuttings and yellow triangle for the measurements of the core) in each well. a- Emmeloord-01 (EMO-01); b- Kampen-01 (KAM-01); c- Nijensleek-01 (NSL-01); d- Sloten-02 (STN-02); e- Wanneperveen-01 (WAV-01). (For interpretation of the references to colour in this figure legend, the reader is referred to the Web version of this article.)

the crust, thickness, and temperature. Lorenz and Nicholls (1984) indicate an increase in magmatism, together with the extrusion of high volumes of basaltic and rhyolitic magmas. In our study area, the sedimentary layers are intruded by sills and dykes, evidenced in the wells Baarlo-01 and De Wijk-07 (van Bergen and Sissingh, 2007). The described extrusive basalt in Steenwijkerwold-1 is also of a similar composition. The extrusive nature of this mafic rock should however be discussed as the basalt dated 291 + - 8Ma is stratigraphically located in the older Ruurlo Fm (~310Ma). We formulate two explanations, the first one is that the felsic rock is not basalt but gabbro (i.e., intrusive), both rocks have the same chemical composition. This first scenario is supported by two arguments (1) the surrounding wells (Baarlo-1 (BRL-01), De Wijk −7 (WYK-07) and Hardenberg-2 (HBG-02)) with magmatism at the same period having being described as Gabbro, and (2) the extrusive description has been made on cuttings (no cores has been taken at this depth). The other explanation is that the K/Ar dating of the basalt is not correct (view also expressed by Sissingh, 2004) and the timing of magmatism is closer to 310 Ma.

The sills, dykes and basaltic rocks have a slightly differentiated composition with a mantle-derived source. The impact of this very low

differentiated magma (dolerite and gabbro) helps to limit the choices of the intrusion's temperature to a relatively high value. The temperature of mafic intrusions is usually accepted as being between 1050 °C and 1250 °C (e.g., Allibon et al., 2011). Annen and Sparks (2002) have discussed the thermal impact of an intrusion and use a temperature of 1100 °C for a wet magma and 1300 °C for a dry magma. Through these studies, we can select a realistic temperature of 1100 °C with a possible variation of ± 200 °C. With the temperature intrusion fixed at 1100 °C, the required thickness is 4000 m and the top of the intrusion is positioned just below the sediments.

Variation in just one of these three parameters (temperature, thickness, or depth) generates a misfit with the VR measurement within the maturation modelling. In Fig. 9 we performed a sensitivity analysis, by varying each parameter one at a time around the values of the main model. The variation in thickness of the intrusion (Fig. 9a) has a strong impact on the modelling (e.g., at 2500 m, an increase of 1000 m causes a VR variation of 0.5%). Moreover, when the thickness of a few thousands meters is reached, depending on the parameters, the maturation modelling shows a plateau at a VR value of 4.66%. The variation of the temperature (Fig. 9b), with a variation step of 100 °C, has a lower
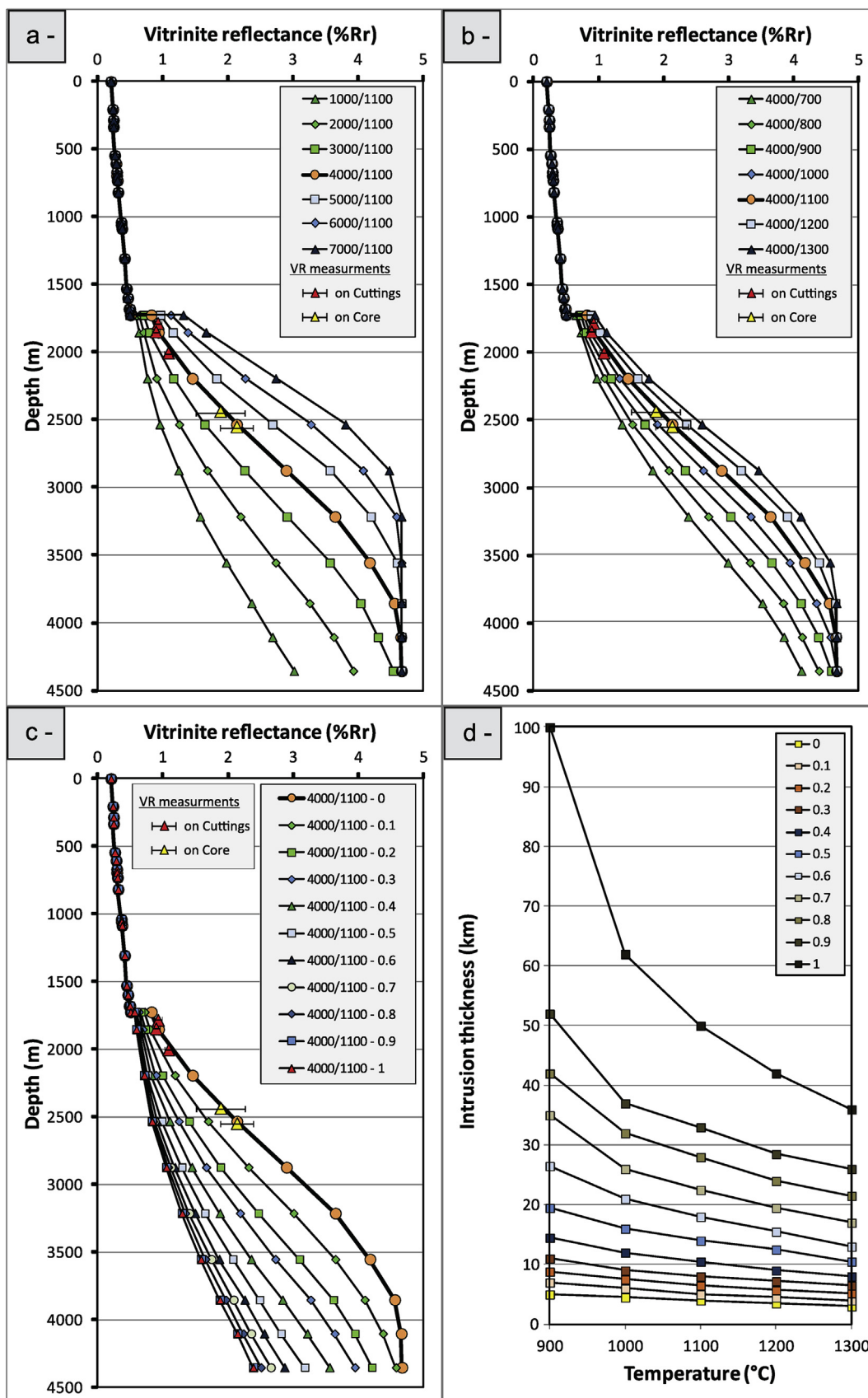
**Fig. 9.** Impact of intrusion parameters on maturation modelling. Standard values for the intrusion are a temperature of 1100 °C, a thickness of 4000 m and a depth of 0 (just below the sediments). Yellow and red triangles represent calibration measurements respectively for core and cuttings. a- Variation in thickness from 1000 m to 7000 m with increasing steps of 1000 m. b- Variation in temperature from 700 °C to 1300 °C, with increasing steps of 100 °C. c- Variation in the depth of the top of the intrusion from 0 (below the base of the sediments) to 1 (base of the lithosphere) with increasing steps of 0.1. d- Variation of all three parameters simultaneously, with all combinations shown fitting the reference measurements. (For interpretation of the references to colour in this figure legend, the reader is referred to the Web version of this article.)

impact on the model than the thickness does. However, a variation of ± 200 °C brings the modelling away from the calibration data. In terms of the depth of the intrusion, the depth is limited; it can only be placed deeper until it is located at the base of the lithosphere and thereafter becomes an underplating body rather than an intrusion. The result (Fig. 9c) indicates a rapid evolution up to the point at which the intrusion is located half way through the lithosphere (i.e., a value of 0.5), after which the impact on the modelling decreases and becomes very limited.

Fig. 9d shows the variation of the three parameters (thickness, temperature, and depth) used in the modelling. In all cases, the modelled VR fit the measurements in Emmeloord-1. In other words, any combination of these three parameters is theoretically valid for our model. The main limitation is connected to geological input. Due to the composition of the surrounding dykes and sills, the temperature is likely to be around 1100 °C. As the figure demonstrates, the isolated intrusive body indicates a single intrusion; in terms of our model, the implication is a limited thickness of around 4000 m.

### 4.3. Timing of the intrusions

The modelled wells predict an elevated maturity depth trend in the Carboniferous section. To test both the timing and regional validity of the model, we selected additional wells in the vicinity of the study area, where a) maturity data indicate anomalously high maturity values in the Carboniferous section and b) VR measurements are available both in the Mesozoic and in the Palaeozoic. Two wells have been identified with these characteristics: Hoogkarspel-2 (HOK-02) and Bakkum-Castricum-1 (BAC-01) (Fig. 2). The Hoogkarspel-2 well is positioned geographically on the south west of the IJsselmeer and geologically in the Noord-Holland Platform. The second well, Bakkum-Castricum-1, is located to the southwest of Hoogkarspel-2, in the Central Netherland Basin. Bakkum-Castricum-1 and Hoogkarspel-2 are modelled using similar boundary conditions, sedimentary and lithospheric parameters, and equivalent tectonic phases as those adopted for the five wells discussed above.

The results of these models are displayed in Fig. 10. Importantly, the two calibrations — tectonic subsidence (Fig. 10a1 and b1) and VR (Fig. 10a2 and b2) — yield good results. The tectonic subsidence for both Hoogkarspel-2 (Fig. 10a1) and Bakkum-Castricum-1 (Fig. 10b1) shows three uplift stages: Early Permian after the Permo-Carboniferous igneous event, Late Jurassic in relation to the North-Sea rifting, and Late Mesozoic in connection with the Alpine orogeny. However, of these stages, only the first one that is linked to the Variscan orogeny and subsequent magmatism is strongly expressed in the heat flow (Fig. 10a1 and b1), and also associated with lithospheric stretching. The combined effect of Variscan orogeny and magmatism is confirmed by the results obtained from the model for the VR (Fig. 10a2 and b2). In the well Hoogkarspel-2 (Fig. 10a2), the deepest VR measurement is at a depth of 1821 m. It shows a slight increase in the VR trend, which is confirmed by the modelled curve. This lowest measurement is from the Permian, while the shallowest measurements are in the Cretaceous. The VR of the Bakkum-Castricum-1 well (Fig. 10b2), reveals a similar trend, with the VR trend in the Carboniferous being higher (although still below 2253 m) compared to the overlying layers. However, Carboniferous magmatic activity is unlikely to have reached this area as the Texel-IJselmeer High has been acting as a boundary (van Buggenum and Den Hartog Jager, 2007).

## 5. Regional context of magmatism

Our model predicts a high volume of widespread Permo-Carboniferous intrusions. This fits with the pervasive nature of Late Carboniferous-Permian regional volcanism in terms of both the driving tectonic context and the features of magma emplacement discussed in previous studies (Neumann et al., 2004; Timmerman, 2004; Torsvik

et al., 2008). Whereas the wider North Sea has seen several periods of intrusive and extrusive magmatism since the Carboniferous at least, notably during the Triassic Jurassic and early Cenozoic, only the Permo-Carboniferous phase of wide-spread plume magmatism caused a thermal anomaly that is recorded throughout the region. The other magmatic events have had little effect due to their limited volume and/or large distance to the study area, the northern onshore Netherlands. The few sills and dykes of Permo-Carboniferous age that have been encountered in wells (e.g. SWD-01, BRL-01, and WYK-07) in the study area have a limited thickness (between 1 and 26 m) and their thermal effect is too insignificant to be recorded by vitrinite reflectance. Shallow sills that have been described in the southern North Sea are known further to the west and have been attributed to the Paleocene magmatic center in Scotland. No such sills have been described in the study area.

Several authors have described the geodynamic context of the mantle plume emplacement that coincided with a change in the stress regime from compressive to wrenching deformation (Ziegler, 1990; McCann et al., 2006) and that triggered magmatism and volcanism in the aftermath of Variscan orogeny throughout north-western Europe (e.g., Lorenz and Nicholls, 1984; Matte, 1986; Ziegler, 1990; Prijac et al., 2000; van Wees et al., 2000; Ziegler et al., 2006). Several examples of magmatic activity that date from around the Permo-Carboniferous boundary have been described in the South Permian Basin. The most extensive magmatism, with volcanic deposits forming a thickness of up 2000m, occurred in the North East German Basin (Benek et al., 1996). The magnitude of this volcanism has been related to a regional weakening caused by changes in the stress regime (Scheck and Bayer, 1999). To the north, the Oslo rift system also shows its first stage of volcanism during the same period (Neumann et al., 2004) and although the extent of this volcanism is difficult to assess, there appears to have been a high level of activity in the central North Sea (e.g., Glennie, 1998). To the west, the British Isles show areas with significant intrusive magmatism for example in Cornwall (southwest England). This extensive evidence of magmatism from the same period, associated with a comparable composition indicating an origin of partial melting of the lithospheric, points firmly in the direction of a large scale thermal perturbation in the lithosphere. The timing of Permo-Carboniferous magmatism varies across northern Europe, ranging from the latest Carboniferous in the UK up to the Permian in the North Sea and Germany (Heeremans et al., 2004).

The importance of the lithospheric structural controls in a spatial partitioning of the Permo-Carboniferous magmatism along the southern margin of the Southern Permian Basin indicates that magmatism in this area is concentrated along the northern margin of the Avalonian plate (Smit et al., 2016). This is in agreement with our results from the TIJH that is located at the edge of Avalonia. Evidence for magmatism away from the Caledonian suture zones is found in the English counties of Shropshire, Derbyshire, and Gloucestershire (Stephenson et al., 2003).

Our model suggests an extensive thickness of intrusions below the sediments. Outcrop data of sills and dykes in northern England (i.e., sills over 90 m thick and dykes up to 65 m thick) and in Scotland (i.e., sills up to 180 m thick and dykes up to 50 m thick and 130 m long), provide an analogue to understanding the intrusive bodies in the bed rocks below the sediments in the Netherlands. This could suggest that the geometry of the intrusion(s) in our area of study is likely to be elongated (i.e., dykes or sills) rather than batholith-shaped. Such an interpretation would also be consistent with the deep faults in our area of interest (e.g. Kombrink et al., 2008; van Buggenum and Den Hartog Jager, 2007; Smit et al., 2018), which could have provided a preferential pathway for the rising magma.

## 6. Conclusions

Tectonic modelling of selected wells shows that tectonic subsidence and exhumation can be reconciled with a significant heat flow pulse, capable of explaining an elevated maturity gradient in Carboniferous
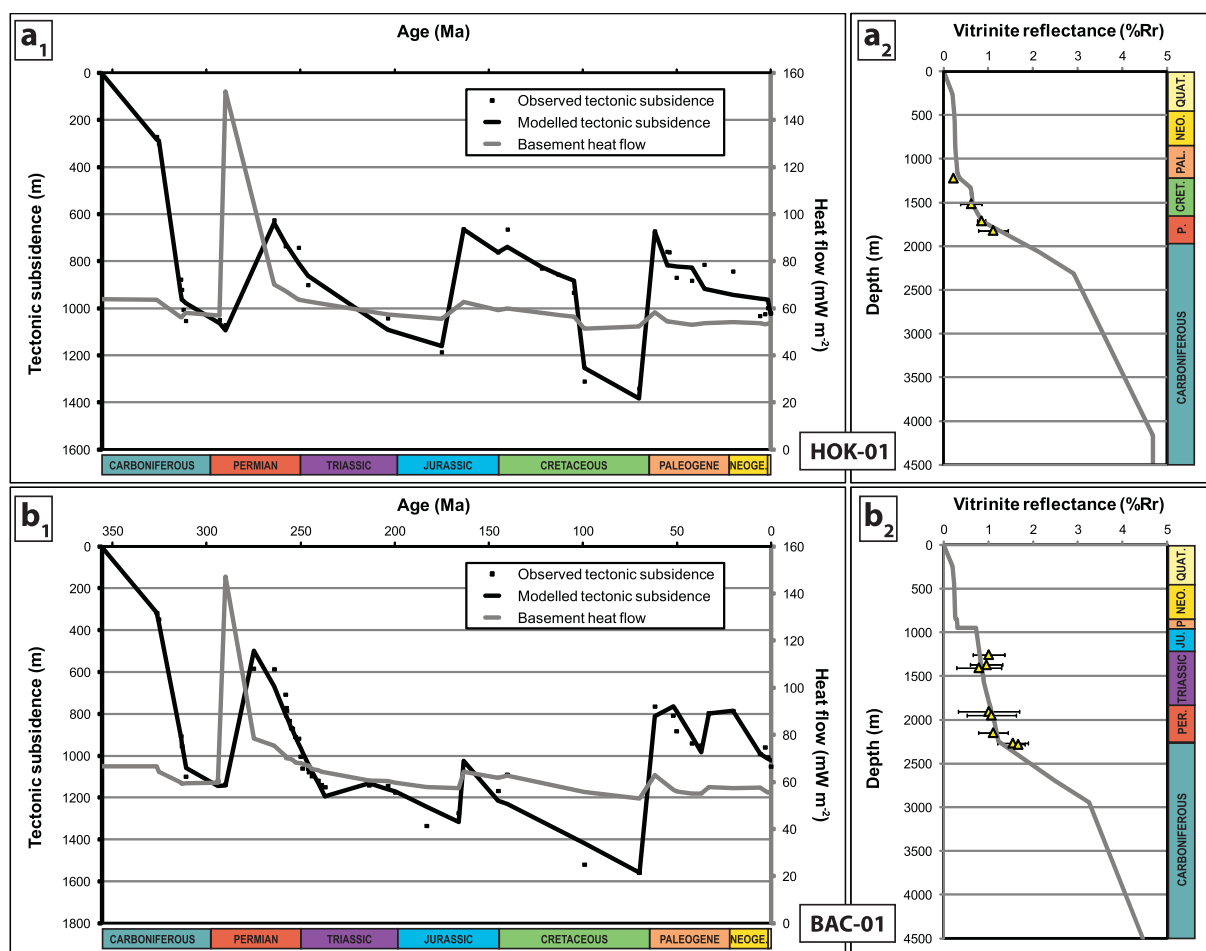
**Fig. 10.** Modelling results of wells: a- Hoogkarspel-2 (HOK-02) and b- Bakkum-Castricum-1 (BAC-01). a1 and b1-tectonic subsidence observed (black dot) and modelled (black curve), and basement heat flow (grey curve). a2 and b2-modelled vitrinite reflectance curve (grey curve) and vitrinite reflectance measurements (yellow triangle) with standard deviation. (For interpretation of the references to colour in this figure legend, the reader is referred to the Web version of this article.)

rocks. The heat flow pulse is related to the emplacement of a post-Variscan mantle plume, which is associated with pervasive mantle upwelling and magmatism. Quantitative assessment of heat flow shows that mantle upwelling and underplating at the base of the crust, as proposed by van Wees et al. (2000, 2009) provides insufficient heat flow to explain strongly elevated maturity-depth trends. Our study demonstrates that widespread intrusion at shallow crustal levels provides an elevated heat flow mechanism with a regional impact, consistent with observed high maturity-depth trends (though our restored heat flow of ca. 125 mW/m$^2$ is slightly higher than the rifting which is ca. 120 mW/m$^2$). The model and maturity data demonstrate that elevated maturity as a consequence of the heat flow pulse can well be into the gas window during the heat pulse, provided that the source rock was buried to a depth of 500–1000 m at the time of the heat pulse and was not eroded during the following exhumation. In our 1D model approach, the adopted spatially uniform geometry of the shallow intrusion should be interpreted with care, as the results of this study demonstrate the intrusions responsible for the heat flow pulse most likely had been marked by more complex 2D/3D geometries importance of heat flow characterization in understanding of compressional to extensional plate tectonics.

## Acknowledgments

## Appendix A. Supplementary data

Supplementary data to this article can be found online at https://doi.org/10.1016/j.marpetgeo.2019.104118.

## References

Allen, P.A., Allen, J.R., 2005. Basin Analysis: Principles and Applications, second ed. Blackwell, Oxford.

Allibon, J., Bussy, F., Lewin, É., Darbellay, B., 2011. The tectonically controlled emplacement of a vertically sheeted gabbro-pyroxenite intrusion: feeder-zone of an ocean-island volcano (Fuerteventura, Canary Islands). Tectonophysics 500, 78–97.

Alves, T.M., Elliott, C., 2014. Fluid flow during early compartmentalisation of rafts: a North Sea analogue for divergent continental margins. Tectonophysics 634, 91–96.

Annen, C., Sparks, R.S.J., 2002. Effects of repetitive emplacement of basaltic intrusions on thermal evolution and melt generation in the crust. Earth Planet. Sci. Lett. 203, 937–955.

Artemieva, I.M., Mooney, W.D., 2001. Thermal thickness and evolution of Precambrian lithosphere: a global study. J. Geophys. Res. 106, 16387–16414.

Ballèvre, M., Bosse, V., Ducassou, C., Pitra, P., 2009. Palaeozoic history of the Armorican Massif: models for the tectonic evolution of the suture zones. Compt. Rendus Geosci. 341, 174–201.

Beglinger, S.E., van Wees, J.D., Cloetingh, S., Doust, H., 2012. Tectonic subsidence history and source-rock maturation in the Campos Basin, Brazil. Pet. Geosci. 18, 153–172.

Bellingham, P., White, N., 2000. A general inverse method for modelling extensional sedimentary basins. Basin Res. 12, 219–226.

Benek, R., Kramer, W., McCann, T., Scheck, M., Negendank, J.F.W., Korich, D., Huebscher, H., Bayer, U., 1996. Permo-Carboniferous magmatism and related subsidence of the NE German Basin. Tectonophysics 266, 379–404.

Bond, G.C., Kominz, M.A., 1984. Construction of tectonic subsidence curves for the early Paleozoic miogeocline, southern Canadian Rocky Mountains: implications for subsidence mechanisms, age of breakup, and crustal thinning. Geol. Soc. Am. Bull. 95, 155–173.

Bonté, D., van Wees, J.-D., Verweij, J.M., 2012. Subsurface temperature of the onshore Netherlands: new temperature dataset and modelling. Neth. J. Geosci. 91, 491–515.

Brown, P.E., Ryan, P.D., Soper, N.H., Woodcock, N.H., 2008. The newer granite problem revisited: a transtensional origin for the early Devonian trans-suture suite. Geol. Mag. 145, 235–256.

Burgers, W.F.J., Mulder, G.G., 1991. Aspects of the late Jurassic and Cretaceous history of The Netherlands. Geol. Mijnb. 70, 347–354.

Burov, E., Cloetingh, S., 2009. Controls of mantle plumes and lithospheric folding on modes of intraplate continental tectonics: differences and similarities. Geophys. J. Int. 178, 1691–1722.

Cloetingh, S., Ziegler, P.A., 2007. Tectonic models for the evolution of sedimentary basins. In: In: Schubert, G. (Ed.), Treatise on Geophysics, vol. 6. pp. 485–611.

Cloetingh, S., van Wees, J.D., Ziegler, P.A., Lenkey, L., Beekman, F., Tesauro, M., Förster, A., Norden, B., Kaban, M., Hardebol, N., Bonté, D., Genter, A., Guillou-Frottier, L., TerVoorde, M., Sokoutis, D., Willingshofer, E., Cornu, T., Worum, G., 2010. Lithosphere tectonics and thermo-mechanical properties: an integrated modelling approach for Enhanced Geothermal Systems exploration in Europe. Earth Sci. Rev. 102, 159–206.

Corver, M.P., Doust, H., van Wees, J.D., Cloetingh, S., 2011. Source-rock maturation characteristics of symmetric and asymmetric grabens inferred from integrated analogue and numerical modeling: the southern Viking Graben (North Sea). Mar. Pet. Geol. 28, 921–935.

Crittenden, S., 1987. The "Albian transgression" in the southern North sea basin. J. Pet. Geol. 10, 395–414.

de Jager, J., 2007. Geological development. In: Wong, Th.E., Batjes, D.A.J., de Jager, J. (Eds.), Geology of the Netherlands. Royal Netherlands Academy of Arts and Sciences, Amsterdam, pp. 5–26.

Doornenbal, J.C., Stevenson, A.G. (Eds.), 2010. Petroleum Geological Atlas of the Southern Permian Basin Area. European Association of Geoscientists & Engineers, Houten, Netherlands, pp. 342.

Fjeldskaar, W., Johansen, H., Dodd, T., Thompson, M., 2003. Temperature and maturity effects of magmatic underplating in the Gjallar Ridge, Norwegian Sea. In: In: Düppenbecker, S., Marzi, R. (Eds.), Multidimensional Basin Modeling, vol. 7. AAPG/Datapages Discovery Series, pp. 71–85.

François, T., Koptev, A, A, Cloetingh, S., Burov, E., Gerya, T., 2018. Plume-lithosphere interactions in rifted margin tectonic settings: inferences from thermo-mechanical modelling. Tectonophysics 746, 138–154.

Gast, R.E., Dusar, M., Breitkreuz, C., Gaupp, R., Schneider, J.W., Stemmerik, L., Geluk, M.C., Geißler, M., Kiersnowski, H., Glennie, K.W., Kabel, S., Jones, N.S., 2010. Rotliegend. In: Doornenbal, J.C., Stevenson, A.G. (Eds.), Petroleum Geological Atlas of the Southern Permian Basin Area. EAGE Publications, Houten, pp. 101–121.

Geluk, M.C., 2005. Stratigraphy and Tectonics of Permo-Triassic Basins in the Netherlands and Surrounding Areas. PhD thesis. Utrecht University 171 pp.

Geluk, M.C., 2007a. Permian. In: Wong, Th.E., Batjes, D.A.J., de Jager, J. (Eds.), Geology of the Netherlands. Royal Netherlands Academy of Arts and Sciences, Amsterdam, pp. 63–83.

Geluk, M.C., 2007b. Triassic. In: Wong, Th.E., Batjes, D.A.J., de Jager, J. (Eds.), Geology of the Netherlands. Royal Netherlands Academy of Arts and Sciences, Amsterdam, pp. 85–106.

Geluk, M.C., Dusar, M., de Vos, W., 2007. Pre-silesian. In: Wong, Th.E., Batjes, D.A.J., de Jager, J. (Eds.), Geology of the Netherlands. Royal Netherlands Academy of Arts and Sciences, Amsterdam, pp. 27–42.

Glennie, K.W., 1998. Lower Permian-Rotliegend. In: Glennie, K.W. (Ed.), Petroleum Geology of the North Sea: Basic Concepts and Recent Advances. Blackwell Science, Oxford, pp. 137–173.

Gradstein, F., Ogg, J., Smith, A. (Eds.), 2004. A Geologic Time Scale 2004. Cambridge University Press, Cambridge.

Heeremans, M., Faleide, J.I., Larsen, B.T., 2004. Late Carboniferous-Permian of NW Europe: an introduction to a new regional map. In: In: Wilson, M., Neumann, E.-R., Davies, G.R., Timmerman, M.J., Heeremans, M., Larsen, B.T. (Eds.), Permo-Carboniferous Magmatism and Rifting in Europe, vol. 223. Geological Society Special Publication, pp. 75–88.

Herngreen, G., Wong, Th.E., 2007. Cretaceous. In: Wong, Th.E., Batjes, D.A.J., de Jager, J. (Eds.), Geology of the Netherlands. Royal Netherlands Academy of Arts and Sciences, Amsterdam, pp. 127–150.

Hirsch, K.K., Scheck-Wenderoth, M., van Wees, J.-D., Kuhlmann, G., 2010. Tectonic subsidence history and thermal evolution of the Orange Basin. Mar. Pet. Geol. 27, 565–584.

Kombrink, H., Besly, B.M., Collinson, J.D., Den Hartog Jager, D.G., Drozdzewski, G., Dusar, M., Hoth, P., Pagnier, H.J.M., Stemmerik, L., Waksmundzka, M.I., Wrede, V., 2010. Carboniferous. In: Doornenbal, J.C., Stevenson, A.G. (Eds.), Petroleum Geological Atlas of the Southern Permian Basin Area. EAGE Publications, Houten, pp. 81–99.

Kombrink, H., Leever, K.A., van Wees, J.D., Van Bergen, F., David, P., Wong, T.E., 2008. Late Carboniferous foreland basin formation and Early Carboniferous stretching in Northwestern Europe: inferences from quantitative subsidence analyses in The Netherlands. Basin Res. 20, 377–395.

Koptev, A., Cloetingh, S., Burov, E., François, T., Gerya, T., 2017. Long-distance impact of Iceland plume on Norway's rifted margin. Sci. Rep. 7, 10408.

Lorenz, V., Nicholls, I.A., 1984. Plate and intraplate processes of Hercynian Europe during the late Paleozoic. Tectonophysics 107, 25–56.

Matte, P., 1986. Tectonics and plate tectonics model for the Variscan belt of Europe. Tectonophysics 126, 329–374.

McCann, T., Pascal, C., Timmerman, M.J., Krzywiec, P., López-Gómez, J., Wetzel, A., Krawczyk, C.M., Rieke, H., Lamarche, J., 2006. Post-variscan (end carboniferous-early Permian) basin evolution in western and central Europe. In: Gee, D.G.,

Stephenson, R.A. (Eds.), European Lithosphere Dynamics. Memoir 32. Geological Society, London, pp. 355–388.

McKenzie, D., 1978. Some remarks on the development of sedimentary basins. Earth Planet. Sci. Lett. 40, 25–32.

Miles, A.J., Woodcock, N.H., Hawkesworth, C.J., 2016. Tectonic controls on post-subduction granite genesis and emplacement: the late Caledonian suite of Britain and Ireland. Gondwana Res. 39, 250–260.

Nance, R.D., Gutiérrez-Alonso, G., Keppie, J.D., Linnemann, U., Murphy, J.B., Quesada, C., Strachan, R.A., Woodcock, N.H., 2012. A brief history of the Rheic Ocean. Geosci. Front. 3, 25–135.

Neumann, E.-R., Wilson, M., Heeremans, M., Spencer, E.A., Obst, K., Timmerman, M.J., Kirstein, L., 2004. Carboniferous-Permian rifting and magmatism in southern Scandinavia, the North Sea and northern Germany: a review. In: Permo-Carboniferous Magmatism and Rifting in Europe, vol. 223. Geological Society of London Special Publications, pp. 11–40.

Ogg, J.G., Ogg, G., Gradstein, F.M., 2008. The Concise Geologic Time Scale. Cambridge University Press, Cambridge.

Pharaoh, T.C., Dusar, M., Geluk, M.C., Kockel, F., Krawczyk, C.M., Krzywiec, P., Scheck-Wenderoth, M., Thybo, H., Vejbak, O.V., van Wees, J.D., 2010. Tectonic evolution. In: Doornenbal, J.C., Stevenson, A.G. (Eds.), Petroleum Geological Atlas of the Southern Permian Basin Area. EAGE Publications, Houten, pp. 25–57.

Pharaoh, T.C., Winchester, J.A., Verniers, J., Lassen, A., Seghedi, A., 2006. The western accretionary margin of the east European Craton: an overview. In: In: Gee, D.G., Stephenson, R.A. (Eds.), European Lithosphere Dynamics, vol. 32. Geological Society Memoirs, pp. 291–311.

Pluymaekers, M.P.D., Kramers, L., van Wees, J.-D., Kronimus, A., Nelskamp, S., Boxem, T., Bonté, D., 2012. Reservoir characterisation of aquifers for direct heat production: methodology and screening of the potential reservoirs for The Netherlands. Neth. J. Geosci. 91 (4), 621–636.

Prijac, C., Doin, M.-P., Gaulier, J.-M., Guillocheau, F., 2000. Subsidence of the Paris Basin and its bearing on the late Variscan lithosphere evolution: a comparison between Plate and Chablis models. Tectonophysics 323, 1–38.

Rijkers, R.H.B., Geluk, M.C., 1996. Sedimentary and structural history of the texel-IJsselmeer high, The Netherlands. In: Rondeel, H.E., Batjes, D.A.J., Nieuwenhuizen, W.H. (Eds.), Geology of Gas and Oil under the Netherlands. Kluwer, Dordrecht, pp. 265–284.

Rijks Geologische Dienst, 1993. Geological Atlas of the Subsurface of The Netherlands, Explanation to Map Sheet V: Sneek-Zwolle. Geological Survey of The Netherlands RGD, Haarlem.

Ross, C.A., Ross, J.R.P., 1987. Late Paleozoic sea levels and depositional sequences. In: In: Ross, C.A., Haman, D. (Eds.), Timing and Depositional History of Eustatic Sequences: Constraints on Seismic Stratigraphy, vol. 24. Cushman Foundation for Foraminiferal Research, Special Publication, pp. 137–149.

Royden, L., Keen, C.E., 1980. Rifting process and thermal evolution of the continental margin of eastern Canada determined from subsidence curves. Earth Planet. Sci. Lett. 51, 343–361.

Scheck, M., Bayer, U., 1999. Evolution of the northeast German Basin inferences from a 3D structural model and subsidence analysis. Tectonophysics 313, 145–169.

Sissingh, W., 2004. Palaeozoic and Mesozoic igneous activity in the Netherlands: A tectonomagmatic review. Geologie en Mijnbouw 83 (2), 113–134.

Smit, J., van Wees, J.-D., Cloetingh, S., 2016. The Thor suture zone: from subduction to intraplate basin setting. Geology 44 (9), 707–710.

Smit, J., van Wees, J.-D., Cloetingh, S., 2018. Early Carboniferous extension in East Avalonia: 350 My record of lithospheric memory. Mar. Pet. Geol. 92, 1010–1027.

Stephenson, D., Loughlin, S.C., Millward, D., Waters, C.N., Williamson, I.T., 2003. Carboniferous and Permian Igneous Rocks of Great Britain North of the Variscan Front. Geological Conservation Review 27. Joint Nature Conservation Committee, Peterborough.

Sweeney, J.J., Burnham, A.K., 1990. Evaluation of a simple model of vitrinite reflectance based on chemical kinetics. Am. Assoc. Pet. Geol. Bull. 74, 1559–1570.

ter Borgh, M.M., Jaarsma, B., Rosendaal, E.A., 2018. Structural Development of the Northern Dutch Offshore: Paleozoic to Present. Paleozoic Plays of NW Europe. A. A. Monaghan, Underhill, J. R., Hewett, A. J. & Marshall, J. E. A.. Geological Society, London, Special Publications, London, pp. 471.

Timmerman, M.J., 2004. Timing, Geodynamic Setting and Character of Permo-Carboniferous Magmatism in the Foreland of the Variscan Orogen, NW Europe, in.

Torsvik, T.H., Smethurst, M.A., Burke, K., Steinberger, B., 2008. Long term stability in deep mantle structure: evidence from the ~300 Ma Skagerrak-centered large igneous Province (the SCLIP). Earth Planet. Sci. Lett. 267, 444–452.

Underhill, J.R., Partington, M.A., 1993. Jurassic thermal doming and deflation in the North Sea: implications of the sequence stratigraphic evidence. Petrol. Geol. Conf. series 4, 337–345.

van Adrichem Boogaert, H.A., Kouwe, W.F.P., 1997. Stratigraphic Nomenclature of The Netherlands, revised and updated by RGD and NOGEPA (compilers). Meded. Rijks Geol. Dienst 50.

van Balen, R.T., Houtgast, R.F., Van der Wateren, F.M., Vandenberghe, J., Bogaart, P.W., 2000. Sediment budget and tectonic evolution of the Meuse catchment in the Ardennes and the Roer Valley rift system. Glob. Planet. Chang. 27, 113–129.

van Bergen, M.J., Sissingh, W., 2007. Magmatism in The Netherlands: expression of the north-west European rifting history. In: Wong, Th.E., Batjes, D.A.J., De Jager, J. (Eds.), Geology of the Netherlands. Royal Netherlands Academy of Arts and Sciences, Amsterdam, pp. 197–221.

van Buggenum, J.M., Den Hartog Jager, D.G., 2007. Silesian. In: Wong, Th.E., Batjes, D.A.J., De Jager, J. (Eds.), Geology of the Netherlands. Royal Netherlands Academy of Arts and Sciences, Amsterdam, pp. 43–62.

van Wees, J.D., 2007. Installation Manual and Getting Started Petroprob Version 1.0.

TNO-NITG, pp. 50.

van Wees, J.D., Beekman, F., 2000. Lithosphere rheology during intraplate extension and compression: inferences from automated forward modelling of subsidence data. Tectonophysics 320, 219–242.

van Wees, J.D., Stephenson, R.A., Stovba, S.M., Shymanovski, S., 1996. Tectonic variation in the Dniepr-Donets Basin from automated modelling of backstripped subsidence curves. Tectonophysics 268, 257–280.

van Wees, J.-D., Stephenson, R.A., Ziegler, P.A., Bayer, U., McCann, T., Dadlez, R., Gaupp, R., Narkiewicz, M., Bitzerg, F., Scheck, M., 2000. On the origin of the southern Permian basin, central Europe. Mar. Pet. Geol. 17, 43–59.

van Wees, J.D., Van Bergen, F., David, P., Nepveu, M., Beekman, F., Cloetingh, S., Bonté, D., 2009. Probabilistic tectonic heat flow modeling for basin maturation: assessment method and applications. Mar. Pet. Geol. 26, 536–551.

Van Wijhe, D.H., 1987. Structural evolution of inverted basins in the Dutch offshore. Tectonophysics 137, 171–219.

Ward, N., Alves, T., Blenkinsop, T., 2016. Reservoir leakage along concentric faults in the Southern North Sea: implications for the deployment of CCS and EOR techniques. Tectonophysics 690, 97–116.

White, N., 1993. Recovery of strain rate variation from inversion of subsidence data.

Nature 366, 449–452.

White, R., Smith, L., Christie, P., Kusznir, N., 2018. Lower-crustal intrusion on the North Atlantic continental margin. Nature 452, 460–464.

Wong, Th.E., 2007. Jurassic. In: Wong, Th.E., Batjes, D.A.J., De Jager, J. (Eds.), Geology of the Netherlands. Royal Netherlands Academy of Arts and Sciences, Amsterdam, pp. 107–125.

Wong, Th.E., Batjes, D.A.J., De Jager, J. (Eds.), 2007. Geology of the Netherlands. Royal Netherlands Academy of Arts and Sciences, Amsterdam.

Wygrala, B.P., 1989. Integrated Study of an Oil Field in the Southern Po Basin, Northern Italy. PhD thesis. Köln University.

Ziegler, P.A., 1990. Geological Atlas of Western and Central Europe, second ed. Shell Internationale Petroleum Maatschappij, The Hague.

Ziegler, P.A., Schumacher, M., Dèzes, P., van Wees, J.-D., Cloetingh, S.A.P.L., 2004. Post-Variscan evolution of the lithosphere in the Rhine Graben area: constraints from subsidence modelling. Geol. Soc. Spec. Publ. 223, 289–317.

Ziegler, P.A., Schumacher, M., Dèzes, P., van Wees, J.-D., Cloetingh, S.A.P.L., 2006. Post-orogenic evolution of the Variscan lithosphere in the area of the European Cenozoic rift system. In: In: Gee, D.G., Stephenson, R.A. (Eds.), European Lithosphere Dynamics, vol. 32. Geological Society Memoirs, pp. 97–112.